Nanoscale

PAPER

View Article Online
View Journal | View Issue

Cite this: *Nanoscale*, 2015, **7**, 1830

Co_3O_4 nanoparticles decorated carbon nanofiber mat as binder-free air-cathode for high performance rechargeable zinc-air batteries†

Bing Li,[a] Xiaoming Ge,[a] F. W. Thomas Goh,[a] T. S. Andy Hor,*[a,b] Dongsheng Geng,[a] Guojun Du,[a,b] Zhaolin Liu,*[a] Jie Zhang,[a] Xiaogang Liu[a,b] and Yun Zong*[a]

Received 10th October 2014,
Accepted 26th November 2014

DOI: 10.1039/c4nr05988c

www.rsc.org/nanoscale

An efficient, durable and low cost air-cathode is essential for a high performance metal-air battery for practical applications. Herein, we report a composite bifunctional catalyst, Co_3O_4 nanoparticles-decorated carbon nanofibers (CNFs), working as an efficient air-cathode in high performance rechargeable Zn-air batteries (ZnABs). The particles-on-fibers nanohybrid materials were derived from electrospun metal-ion containing polymer fibers followed by thermal carbonization and a post annealing process in air at a moderate temperature. Electrochemical studies suggest that the nanohybrid material effectively catalyzes oxygen reduction reaction *via* an ideal 4-electron transfer process and outperforms Pt/C in catalyzing oxygen evolution reactions. Accordingly, the prototype ZnABs exhibit a low discharge–charge voltage gap (*e.g.* 0.7 V, discharge–charge at 2 mA cm^{-2}) with higher stability and longer cycle life compared to their counterparts constructed using Pt/C in air-cathode. Importantly, the hybrid nanofiber mat readily serves as an integrated air-cathode without the need of any further modification. Benefitting from its efficient catalytic activities and structural advantages, particularly the 3D architecture of highly conductive CNFs and the high loading density of strongly attached Co_3O_4 NPs on their surfaces, the resultant ZnABs show significantly improved performance with respect to the rate capability, cycling stability and current density, promising good potential in practical applications.

1 Introduction

Metal-air batteries (MABs) stand at the central stage of energy storage research thanks to their promise of extremely high specific energy densities.[1–10] Li-air and Zn-air batteries (ZnABs), the two most studied MABs, are anticipated to deliver theoretical specific energy densities of 3500 and 2500 Wh kg^{-1}, which are 9 and 6 times as high as that of the best reported lithium-ion battery (LIB),[3,8,9] respectively. Apart from using a pure metal anode, such high specific energy densities are attributed to the use of oxygen (O_2) in air as cathode, enabling great reduction in cathode size and overall weight of the batteries. To make rechargeable MABs work, one requires an air cathode of high surface area arising from porous structure with appropriate pore sizes that allows fast diffusion of gaseous O_2 yet avoids the leakage of the electrolyte, and high catalytic activities provided by bifunctional catalysts toward oxygen reduction reaction (ORR) and oxygen evolution reaction (OER) in discharging and charging processes, respectively. To date, catalysts of noble metals and their alloys,[11,12] transition metal-based carbon materials[13,14] and their hybrids,[15–20] have been extensively explored to address the sluggish kinetics of ORR and OER. Cobalt-based nanoparticles (NPs) decorated N-doped carbon materials stand out due to their superior catalytic performances.[16,18,21,22] Dai *et al.* reported cobalt oxide (CoO) on N-doped carbon nanotube (N–CNT)[21] and Co_3O_4 on N-doped graphene (N–G)[22] with comparable ORR activity but superior OER catalytic activity if taking commercial Pt on carbon (Pt/C) as the benchmark. Chen *et al.* constructed 3D crumpled graphene decorated by CoO nanoparticles with high catalytic activities toward both ORR and OER.[18] Despite these promising results, their practical applications are hindered by

[a]*Institute of Materials Research and Engineering, A*STAR (Agency for Science, Technology and Research), 3 Research Link, Singapore 117602, Republic of Singapore. E-mail: zl-liu@imre.a-star.edu.sg, y-zong@imre.a-star.edu.sg*
[b]*Department of Chemistry, National University of Singapore, 3 Science Drive 3, Singapore 117543, Republic of Singapore. E-mail: andyhor@nus.edu.sg*

† Electronic supplementary information (ESI) available: TGA curves of as electrospun Co(II)–PAN fiber and C–CoPAN900; EDX and XPS spectra of the C–CoPAN900; photo of a home-built Zn-air cell and the preparation method of conventional catalyst electrode; polarization curves and corresponding power density plots of the battery using conventional type cathode of C–CoPN900 and commercial Pt/C catalyst; the electrocatalytic properties of hybrid CNFs obtained from varied weight ratios of PAN to cobalt acetate, *e.g.* 16 : 1 and 8 : 1, and their corresponding TGA curves; a comparison of the Zn-air battery performance of this work with recent literatures. See DOI: 10.1039/c4nr05988c

the high cost and low yield of N–CNT and sophisticated fabrication of N–G. There is a pressing need for the development of low cost, simple and scalable methods to produce highly efficient bifunctional catalysts for practical applications.

For air-cathode fabrication, the catalyst is normally loaded onto a porous current collector, *e.g.* a piece of carbon fiber paper,[6] through the casting of a slurry mixture comprising powder catalyst, a conductive matrix (*e.g.* acetylene black,[23,24] Ketjen black,[25,26] or Super P[27]) to improve the conductivity of the electrode,[11,28] and polymeric binder (*e.g.* polytetrafluoroethylene,[9,24] and Nafion[6,29]) to hold all components together. However, these additives not only complicate the preparation procedure but also lead to a weight increase of about 10–40 wt% in the final electrode. Moreover, the incorporation of an insulating polymeric binder increases the contact resistance at the interface of the catalyst and the current collector, thereby retarding the electron transfer.[23] An integrated binder-free air cathode with good conductivity and high catalytic activities will be able to circumvent these issues comfortably. Some recent reports unambiguously demonstrated high performance metal-air/O_2 batteries enabled by such integrated binder-free electrodes.[28,30–35] Zhou *et al.* employed a piece of multi-walled carbon nanotube (MWCNT) paper as a binder-free and additive-free air cathode for Li–O_2 batteries, and the battery exhibited a capacity as high as 34 600 mA h g^{-1}.[30] They further modified the MWCNTs with Ru NPs catalyst and used it as an integrated air cathode, whereby the resultant Li–O_2 batteries exhibited a considerably lower charge overpotential and higher round-trip efficiency.[31] Wang and co-workers investigated air cathodes of MnO_2-coated carbon papers for rechargeable Li–O_2 batteries, and concluded that carbon paper with directly grown MnO_2 as a binder-free air cathode greatly improves the reversibility and cycling stability in battery performances as compared to the air cathode of carbon paper coated with MnO_2 and binder.[33] Similar improvement was observed in ZnABs using an integrated binder-free electrode. Chen *et al.* reported ZnABs using Co_3O_4 nanowires directly grown on a stainless steel mesh as an air cathode enables 1500 discharge/charge cycles of batteries without a notable change in their discharge and charge potentials. In contrast, the conventional air cathode of Co_3O_4 nanowires with a binder shows a significant potential loss after 100 cycles under the same testing parameters.[35]

In this contribution, we present a facile method for fabricating integrated air cathodes using catalyst NPs decorated carbon nanofibers (CNFs) obtained from the electrospinning of a mixture solution comprising selected polymer and metal salt precursors, followed by a simple thermal treatment to carbonize the polymers and convert metal precursor into metal NPs. A post annealing in air at moderate temperature converts metal NPs to the desired metal oxide NPs. The results of the electrochemical investigations reveal good catalytic activity of particles-on-fiber hybrids toward ORR that favours a 4-electron transfer process, and high catalytic activity toward OER, which outperforms commercial Pt/C catalyst in alkaline aqueous electrolyte. The prototype Zn-air rechargeable batteries constructed using such NP-CNF hybrids catalyst showed lower overpotential and good cycling stability. More importantly, we demonstrate that the NP-CNF mat can readily serve as a free-standing air cathode with no requirement of any further modifications. Due to the highly efficient catalytic activities and structural advantages of such an electrode, the ZnAB shows higher current rate capability, better cycling stability and the ability to deliver greater energy density (about 3–4 times) than their counterparts prepared using the conventional slurry method.

2 Results and discussion

2.1 Fabrication and characterization of Co_3O_4 NPs decorated CNFs

The regularity in the molecular structure of polyacrylonitrile (PAN) and the ease of its carbonization made it a popular polymer precursor for the preparation of high conductivity carbon fibers.[28,36,37] The nitrogen-rich PAN (up to ~14.3 at%) provides a good N-source to form N-doped carbon materials, which is proven as an efficient approach to improve the ORR reactivity of carbon-based materials.[38–40] On the other hand, cobalt-based nanomaterials are known as good OER catalysts,[14,21,22] and their integration with N-doped carbon materials tends to further improve the catalytic activity *via* synergetic effects.[22,38,41–43] In light of this, we proposed to synthesize Co_3O_4 NPs-decorated carbon nanofibers as potential efficient bifunctional oxygen catalysts *via* the electrospinning technique using a homogeneous solution of PAN and cobalt acetate in dimethylformamide (DMF) as the starting materials, as schematically illustrated in Fig. 1A. The electrospun Co(II)-containing PAN fibers exhibit a white to pinkish appearance

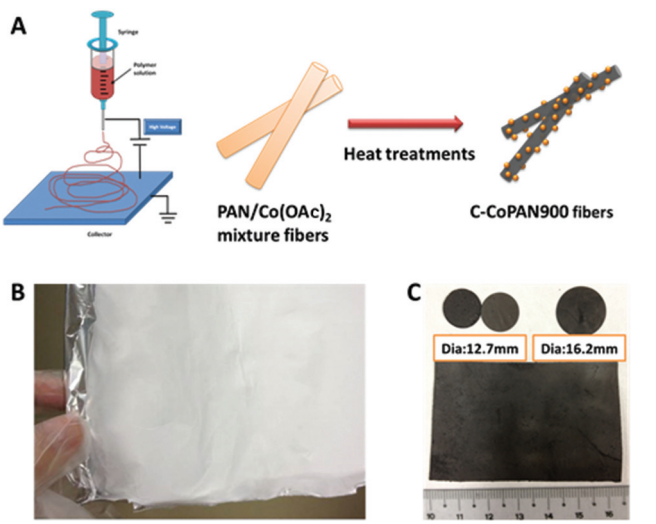

Fig. 1 (A) Schematic illustration of the synthetic strategy for C–CoPAN hybrid catalyst nanofibers. (B) A representative image of the electrospun PAN nanofibers collected on a piece of aluminum foil. (C) A representative image of free-standing carbonized electrospun nanofibers, C–CoPAN, in the shape of discs or rectangles.

(Fig. 1B), depending on the content of cobalt acetate in the starting mixture solution. As these fibers are thermally treated at 900 °C under an inert atmosphere, blackish conductive carbon nanofibers (CNFs, Fig. 1C) with evenly distributed cobalt-based NPs on their surfaces are yielded. An annealing process at 200 °C in air over 90 min converts these surface bonded NPs to cobalt oxides nanoparticles.[23]

Representative SEM images of the carbonized fibers of pure PAN (denoted as C–PAN900) and Co(II)–PAN (denoted as C-CoPAN900) are shown in Fig. 2A and B, respectively. In contrast to C-PAN900 with fibers of approximately 300 nm thick and smooth surfaces, the fibers of C-CoPAN900 are slightly thicker with their surfaces being homogeneously covered by significant amount of nanoparticles (NPs), which are probably derived from the decomposition of Co(II) complexes during the carbonization process. The size of the NPs ranges from 5 to 50 nm, as revealed by the TEM image shown in Fig. 2C. The Raman spectrum (Fig. 2D) of C-CoPAN900 suggests a composition of cobaltosic oxide (Co_3O_4), where 4 of its characteristic peaks at 463, 505, 606, and 673 cm^{-1} corresponding to the E_g, F_{2g}^1, F_{2g}^2 and A_g^1 modes of crystalline Co_3O_4,[40,44] respectively, are clearly observed. In addition, two distinct peaks at 1334 cm^{-1} and at 1579 cm^{-1} are visible in both C-CoPAN900 and C-PAN900, corresponding to the defect induced D-band and graphitic G-band of the carbonaceous material.[37,45] These results indicate the complete conversion of electrospun polymeric NFs to conductive CNFs, and no noticeable changes were induced to the structure of CNFs upon annealing at 200 °C in air. Thermogravimetric analysis (TGA) of C–CoPAN900 (Fig. S1A, ESI†) shows the presence of Co_3O_4 in C–CoPAN900 at as high as 15.7 wt%. The significantly larger content of Co_3O_4 (in comparison to the 8.2 wt% in the Co(II)-PAN fibers prior to the carbonization, Fig. S1B, ESI†) suggests a partial decomposition of the PAN polymer in the NFs as it undergoes the carbonization process, despite the controlled heating under an inert environment.

Energy dispersive X-ray spectroscopy (EDS) analysis proves the co-existence of C, N, O and Co in C–CoPAN900 fibers (Fig. S2, ESI†). The clear N signals in the EDX (Fig. S2, ESI†) suggest the retention of N atoms in the electrospun nitrogen-rich fibers following the high temperature carbonization. X-ray photoelectron spectroscopy (XPS) survey scans unambiguously show the C1s, N1s and O1s peaks (Fig. S3A, ESI†), and the presence of Co_3O_4 is evidenced *via* a detailed scan of Co2p (Fig. S3B, ESI†).[23,46] A detailed investigation that conclusively distinguished different types of cobalt oxides and revealed their interactions with the underlying single sheet of N-doped graphene can be referred to a recent report by Wang and Zhou *et al.*, in which spatially resolved X-ray absorption near edge structure (XANES) spectroscopy and chemical imaging were employed as the main approaches.[41]

High resolution N1s spectrum and the fitting curves (Fig. 2E) reveal the co-existence of two main types of nitrogen in C–CoPAN900, *i.e.* the quaternary nitrogen at 401.2 eV and pyridinic nitrogen at 398.5 eV with concentration of 3.5 at% and 1.9 at%, respectively.[19,45,47,48] The notably decreased nitrogen content after carbonization is attributed to the partial decomposition of PAN, which is consistent with the TGA results. Both quaternary nitrogen and pyridinic nitrogen can serve as active sites for ORR,[39,42,43,48] and quaternary nitrogen is believed to favor the 4-electron transfer process.[49] As the C–CoPAN900 fiber hybrids contain a total N content of up to 5.4 at% with a high proportion of quaternary N (Fig. 2E and F), it is anticipated to deliver excellent ORR catalytic activity. Moreover, the large amount of Co_3O_4 NPs decorated on the C–CoPAN900 fiber surfaces would equip this hybrid material with superior OER catalytic activity. Inheriting the merits of Co_3O_4 NPs and N-doped CNFs together with a possible synergetic effect between both,[16,22,38,41–43] C–CoPAN900 nanofibers are likely to promise a highly efficient bifunctional catalyst.

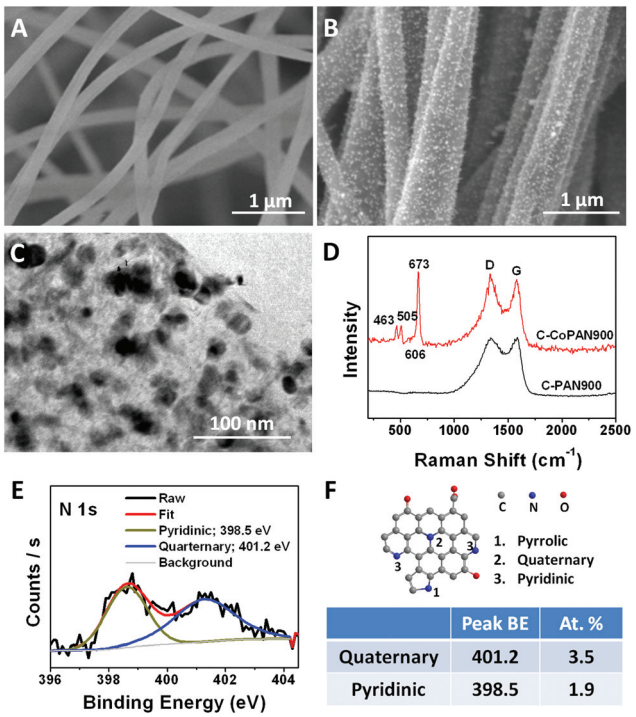

	Peak BE	At. %
Quaternary	401.2	3.5
Pyridinic	398.5	1.9

Fig. 2 (A) A representative SEM image of C–PAN900. (B) A representative SEM image of C–CoPAN900. (C) A representative TEM image of a single nanofiber in C–CoPAN900. (D) Raman spectra of C–PAN900 (black) and C–CoPAN900 (red) with 4 of the characteristic peaks of crystalline Co_3O_4 clearly visible in the latter. (E) High resolution XPS spectrum of N1s for C–CoPAN900. (F) Schematic illustration of the different N atoms doped in carbon matrix. The table summarizes the peak positions as well as the atomic percentages of quaternary–N and pyridinic–N detected in C–CoPAN900.

2.2 Electrochemical properties of Co_3O_4 NPs-decorated CNFs

Cyclic voltammetry (CV) and linear sweep voltammetry (LSV) combined with a rotating disk electrode (RDE) were employed to investigate the catalytic activity of C–CoPAN900 in 0.1 M KOH electrolyte at room temperature using a three-electrode system. The CV curves of C–CoPAN900 in an electrolyte saturated with O_2 or N_2 are presented in Fig. 3A. One can see a clear cathodic reduction peak at about −0.23 V (*vs.* Ag/AgCl) in

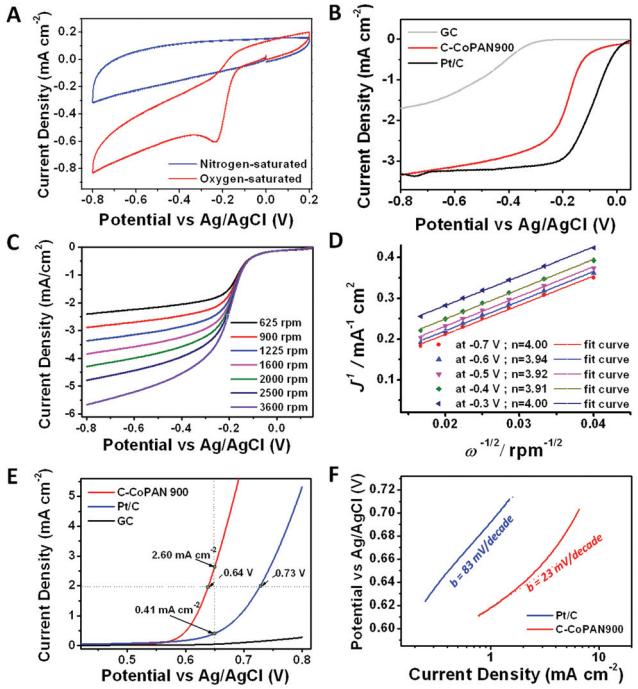

Fig. 3 Electrocatalytic performances of C–CoPAN900. (A) CV curves of C–CoPAN900 in O_2– (red) and N_2– saturated (blue) 0.1 M KOH solution. (B) LSV curves of C–CoPAN900 as compared to GC and Pt/C for ORR catalytic activity at electrode rotating speed of 900 rpm. (C) RDE curves of C–CoPAN900 at rotating rates ranging from 625 to 3600 rpm. (D) Corresponding Koutecky–Levich plots derived from the RDE curves in (C). (E) LSV curves of C–CoPAN900 as compared to GC and Pt/C for OER catalytic activity at an electrode rotating speed of 900 rpm. (F) Tafel slopes of C–CoPAN900 and Pt/C derived from (E). The scan rate was maintained at 50 mV s^{-1} for CVs and 5 mV s^{-1} for all the LSV and RDE tests.

the presence of O_2, which does not exist under a pure N_2 atmosphere, confirming the ORR catalytic activity of C–CoPAN900. Fig. 3B presents the LSV data of C–CoPAN900 together with a bare glassy carbon (GC) electrode and commercial Pt/C (20 wt% Pt on carbon black) obtained at a rotation speed of 900 rpm. C–CoPAN900 exhibits significant improvement in ORR reactivity as compared to GC in terms of the onset potential and current density. The half-wave potential ($E_{1/2}$) of C–CoPAN900 is about −0.188 V, which is just 96 mV more negative than that of the Pt/C catalyst. The current densities between −0.6 to −0.8 V are comparable to those of the Pt/C, suggesting high ORR activity of this fiber hybrid.

RDE measurements were performed at various rotation rates between 625 rpm to 3600 rpm (Fig. 3C) to understand the ORR kinetics of C–CoPAN900. The corresponding Koutecky–Levich (K–L) plots are given in Fig. 3D. The linearity and near parallelism of the fitting lines suggest a first-order reaction kinetics towards the concentration of dissolved O_2 [18,22] for C–CoPAN900 and similar electron transfer number (n) for ORR within a relatively wide electrochemical window. From the K–L equation, the n was calculated to be approximately 4.0 at the potentials between −0.3 to −0.7 V (*cf.* experimental section for the details), suggesting a 4-electron transfer process for C–CoPAN900, which is similar to the benchmark ORR catalyst of commercial Pt/C.

The pronounced OER catalytic activity of C–CoPAN900 is evidenced by the LSV curves (Fig. 3E), where C–CoPAN900 displays a less positive onset potential and significantly larger current density as compared to commercial Pt/C. For example, at a current density of 2 mA cm^{-2} the potential (*vs.* Ag/AgCl) of C–CoPAN900 is 0.64 V, which is about 90 mV less positive as compared to Pt/C (0.73 V). At the potential of 0.65 V, the current density of C–CoPAN900 is up to 2.60 mA cm^{-2}, which is about 6 times greater than that of Pt/C (0.41 mA cm^{-2}) at the same potential. The superior OER performance of C–CoPAN900 was further supported by its small Tafel slope of 23 mV per decade, which is less than 1/3 of that of Pt/C (83 mV per decade), as shown in Fig. 3F.

The outstanding catalytic activities of C–CoPAN900 toward both ORR and OER prove it as an efficient bifunctional oxygen catalyst. The bifunctional catalytic activities may be attributed to the high content of ORR active N-"doping" (quaternary nitrogen and pyridinic nitrogen) and the large amount of OER active Co_3O_4 NPs; however, as the N sites in carbonaceous materials are found to be the primary covalent anchoring sites for the transition metal oxides, the availability of free nitrogen sites in such hybrid material will be limited, which thereby compromises its contribution to the ORR activity. In this case, good ORR activity may have a notable contribution from a synergetic effect between the active N-sites and the adjacent Co_3O_4 NPs, with the possibility of even a dominant contribution from such "covalently" bonded Co_3O_4 NPs on the basis of the proven oxidation and reduction capability of octahedral Co(III).[41] Such a synergetic effect between Co oxides and N-doped graphitic carbons has been thoroughly investigated and proven using X-ray absorption near edge structure (XANES) spectroscopy.[16,22,41] As the C–CoPAN900 in this work possesses Co_3O_4 NPs and N-doped graphitic carbon, it is reasonable to assume the existence of a similar synergetic effect between the Co_3O_4 NPs and adjacent N-sites on the nanofibers. Nevertheless, further studies using XANES spectroscopy on our C–CoPAN900 system may provide in-depth understanding on such a synergistic effect and its mechanism, guiding the design of new bifunctional oxygen catalyst to further improve the catalyst performance. This is part of our ongoing work.

2.3 ZnABs using air-cathode of Co_3O_4 NPs-decorated CNFs slurry

The small diameter of these carbon nanofibers that provides large interfaces between the catalytically active sites and the electrolyte, as well as the direct attachment of Co_3O_4 that shortens the electron transfer distance and reduces contact resistance are clearly structural advantages. Such structural advantages and high catalytic activity toward ORR and OER make C–CoPAN900 a promising material as a catalyst cathode for MABs. In accordance, the battery performance of C–CoPAN900 was tested. Rechargeable ZnABs were constructed using C–CoPAN900 as the catalyst air-cathode in a home-built

battery cell, in which a polished Zn plate serves as the anode with an alkaline aqueous electrolyte consisting of 6 M KOH and 0.2 M $ZnCl_2$ (Fig. 4A). To prepare the catalyst air-cathode, two different strategies were adopted separately. One involved using the conventional slurry method in which the pre-formulated slurry comprising the catalyst and the necessary additional ingredients was applied onto a piece of porous carbon paper (*cf.* experimental section, and Fig. S4, ESI†); the other method involved employing a C–CoPAN900 nanofiber mat (Fig. 1C) directly as an integrated electrode that served as both a catalyst air cathode and a current collector in the ZnAB. An air cathode using the commercial Pt/C as the catalyst was prepared for comparison purposes.

Fig. 4B shows the galvanostatic discharge–charge curves of ZnABs with air-cathode of C–CoPAN900 or Pt/C, respectively, prepared by the conventional slurry method. At a low current density of 1 mA cm^{-2} with a discharge–charge period of 30 min for each state, the ZnAB with C–CoPAN900 air-cathode displays a discharging voltage of 1.26 V, which is comparable to that of Pt/C, but a charging voltage of 1.96 V, which is significantly lower than that of Pt/C (2.09 V) tested under the same conditions. These results show that C–CoPAN900 outperforms Pt/C by comparable ORR catalytic activity and superior OER catalytic activity, which is in agreement with the conclusions from the results of the electrochemical studies.

Impressively, after discharge–charge testing for a continuous 135 cycles (equivalent to 135 h), a slight increase of 0.08 V (from 0.70 V to 0.78 V) was observed for the voltage gap between the charging and discharging of ZnAB with air-cathode of C–CoPAN900. The energy efficiency[6] was calculated to be about 64.0% at the initial stage and maintained at 61.4% after prolonged cycling. In contrast, ZnAB with a Pt/C-based air-cathode shows notable changes in both discharge and charge voltage, *i.e.* from 1.26 V down to 1.21 V for discharge and from 2.09 V up to 2.3 V for charge, respectively. The voltage gap increases by 0.26 V and the energy efficiency drops from 60.2% to 52.6%.

As the testing current density was increased to 2 mA cm^{-2} and the ZnAB was cycled over a longer period (25 h for each discharge and charge segment), again the voltage change was considerably smaller for the C–CoPAN900 air-cathode. The voltage gap remained at about 0.9 V after continuous testing for more than 250 h, the energy efficiency remained at about 56.3% (Fig. 4C). In sharp contrast, ZnABs with Pt/C-catalyst based cathode quickly hit the cut off voltage of 2.6 V during charging, revealing the inability to be efficiently charged even at its first cycle (Fig. 4D). This further confirms the superior bifunctional catalytic activity and stability of C–CoPAN900 in an alkaline aqueous electrolyte over Pt/C.

2.4 ZnABs using integrated air-cathode of binder-free Co_3O_4 NPs-decorated CNFs mat

Encouraged by the abovementioned promising findings, we further evaluated the battery performance of ZnAB using C–CoPAN900 mat as an integrated catalyst air-cathode. Fig. 5A shows a typical polarization curve (*V*–*i*) and the corresponding

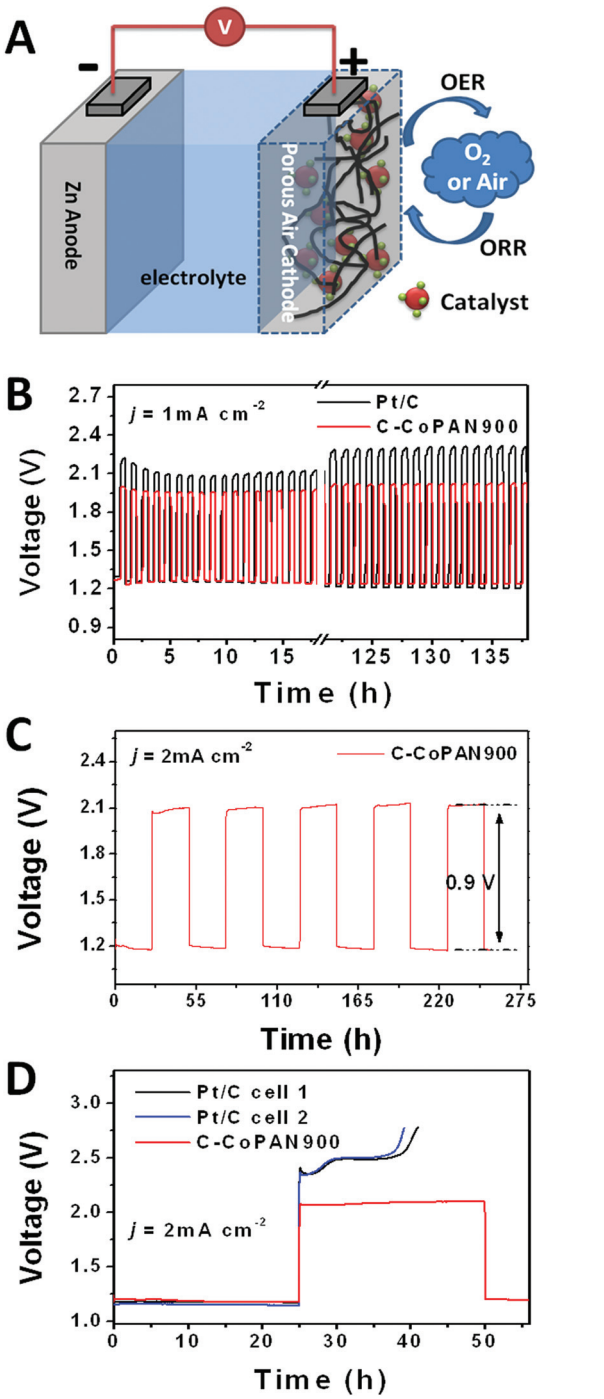

Fig. 4 (A) A schematic illustration of a ZnAB consisting of a Zn anode, alkaline electrolyte and a drop-cast cathode prepared by dropping the active material suspension onto a porous current collector, *e.g.* carbon paper. (B) Discharge–charge cycling of ZnABs using C–CoPAN900 (red) or Pt/C (black) based cathode at a current density of 1 mA cm^{-2} with cycle periods of 30 min discharge and 30 min charge per cycle. (C) Cycling performance of ZnABs using a C–CoPAN900 based cathode at 2 mA cm^{-2} in long cycle periods of 25 h for each discharge and charge segments. (D) Cycling performance of ZnAB at 2 mA cm^{-2} in long cycle periods (50 h per cycle) using C–CoPAN900 (red curve) or commercial Pt/C based cathode (black and blue curves for cell one and cell two, respectively). Similar behavior of Pt/C in two separate cells confirms the poor rechargeability of the Pt/C catalysts rather than a random measurement error.

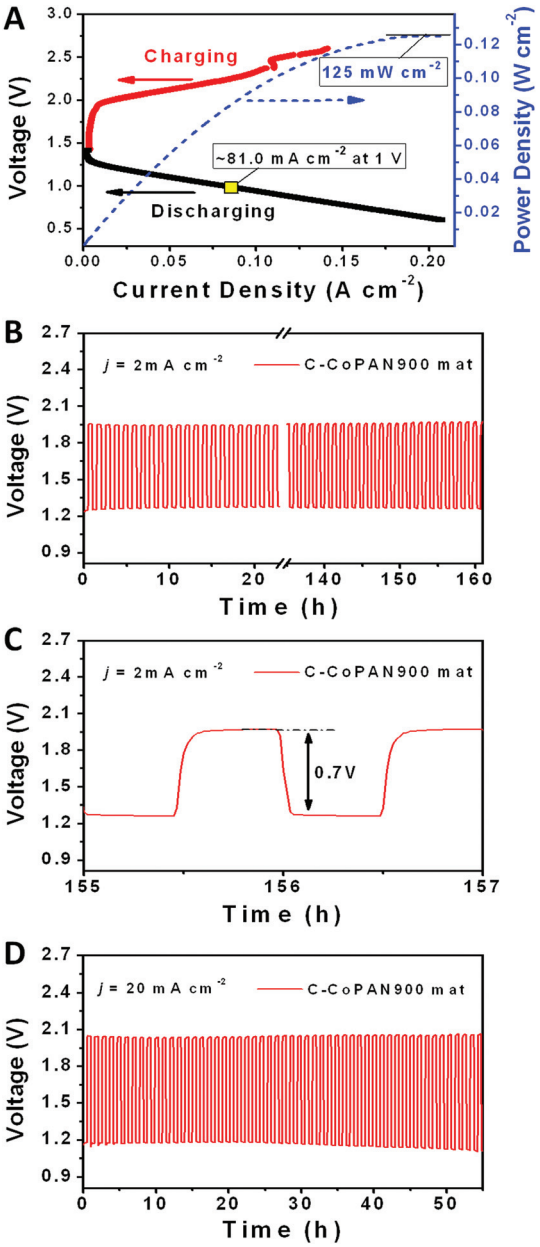

Fig. 5 Battery performance of Zn-air cell constructed using C–CoPAN900 mat directly as an integrated catalyst cathode. (A) Discharge and charge polarization curves (*V*–*i*) of the battery and their corresponding power density plot. (B) Cycling performances of the ZnAB at moderate current density of 2 mA cm^{-2}. (C) A selected cycle in (B) to show the details. (D) Cycling performances of the ZnAB at a high current density of 20 mA cm^{-2}.

power density plot of such ZnAB. Remarkably, this integrated catalyst electrode of C–CoPAN900 mat exhibits a significant improvement in the battery performance in terms of current density and peak power density. At the discharging voltage of 1 V, the C–CoPAN900 integrated catalyst electrode delivers a current density of up to ~81.0 mA cm^{-2}, which is about 6 times as high as that of the C–CoPAN900 electrode prepared using the conventional slurry method (12.3 mA cm^{-2}, Fig. S5, ESI†). The peak power density of the ZnAB with the C–CoPAN900 mat air-cathode reaches 125 mW cm^{-2}, which is about 5 times as high as that of ZnAB with the conventional C–CoPAN900 air-cathode (29 mW cm^{-2}, Fig. S5, ESI†). The power density and peak power density of ZnAB with integrated C–CoPAN900 mat air-cathode are also higher than those in the previously reported works (Table S1, ESI†).[14,50–52]

Fig. 5B presents typical cycling results of the ZnAB at 2 mA cm^{-2} (1 h per cycle) using an integrated air-cathode of C–CoPAN900 mat. Unsurprisingly, this ZnAB clearly outperforms the one with an air-cathode of the same active material but loaded *via* the conventional slurry method (Fig. 4C). One observes superior cycling stability with a smaller voltage gap, and no distinguishable voltage drop in discharging or voltage rise in charging is visible and the voltage gap is stabilized at ~0.7 V, even after continuous cycling of more than 160 cycles (Fig. 5B and C). Benefited from the reduced voltage gap of about 0.2 V (comparing Fig. 5C and Fig. 4C), the energy efficiency of the battery is improved to 65.4% as compared to that of the ZnAB with the conventional C–CoPAN900 air-cathode (56.3%). It is worth highlighting that the C–CoPAN900 mat also enables the ZnAB to operate at an even higher current rate with high stability, as demonstrated in Fig. 5D. At a current density as high as 20 mA cm^{-2} at 1 h per cycle, the initial discharge and charge voltages were about 1.19 V and 2.04 V, respectively, with a voltage gap of only about 0.85 V. After cycling for 55 cycles, the increase in voltage gap was merely about 0.09 V. This battery performance is considerably better than what has been reported previously (Table S2, ESI†).[14,25,53]

Clearly, apart from the high catalytic activity of C–CoPAN900, significant improvement in the battery performance in terms of power density, high rate capability and recharging stability is also due to the structural merits of the integrated electrode. Firstly, the direct attachment of Co_3O_4 NPs onto conductive carbon nanofibers in the absence of polymeric binders and additional conductive agent effectively reduces the contact resistance and shortens the electron transfer pathway. Secondly, with Co_3O_4 NPs firmly bound to the carbon nanofibers, the possibility of agglomeration or detachment of these active NPs during cycling test is mitigated and majority of the catalytically active sites are retained. As a clear contrast, agglomeration of NPs is often found in electrodes using NPs prepared from the conventional methods.[28] Moreover, the interconnected 3D architecture of CNF network provides a large area of electrolyte/nanofiber interfaces and interstices between the fibers, thus enabling rapid ion transport and fast oxygen diffusion.

3 Conclusions

In summary, an integrated catalyst electrode that enables high performance rechargeable ZnABs is presented. The bifunctional catalytically active Co_3O_4 NPs decorated carbon nanofibers are prepared by electrospinning with subsequent heat

treatment, and eventually made freestanding and directly used as an air cathode that is free of polymeric binders, conductive additives and additional current collectors. Electrochemical investigations reveal that Co_3O_4 NPs decorated carbon nanofibers are efficient bifunctional oxygen catalysts with 4-electron transfer behaviour toward ORR and superior performance toward OER. Due to their highly efficient catalytic activity and structural merits, the hybrid C–CoPAN900 nanofiber mat as an integrated air-cathode shows significantly improved ZnAB performance with respect to the current rate capability, cycling stability and energy density, suggesting this type of integrated electrode holds great promise for the development of high power and high energy density MABs.

4 Experimental

4.1 Material synthesis

The hybrid CNF material of C–CoPAN900 was synthesized by combining electrospinning technique[28,29,32,37,54–56] with a subsequent heat treatment. The precursor solutions used for electrospinning were prepared by dissolving PAN and cobalt acetate in dimethylformamide (DMF) in a typical weight ratio of 4 : 1 under magnetic stirring for over 10 h to ensure the homogeneity of the two-component mixture. The resultant precursor with ~10 wt% of PAN in DMF was loaded into a 10 mL syringe with a 22-gauge blunt tip needle that was subsequently mounted onto a syringe pump (KD Scientific, KDS 100, USA) with flow rate control. The electrospinning was conducted by applying a positive voltage of 19 kV between the needle and the grounded aluminum foil separated by a distance of ~20 cm.[28,29,32,54] The electrospun nanofibers were collected using a piece of aluminum foil. As a control, blank PAN fiber was electrospun from pure PAN solution of ~10 wt% in DMF. For carbonization, the as-prepared fibers were first stabilized in air at 260 °C for 1 h and then heated in a N_2 environment at a temperature ramp of 5 °C per min to 900 °C and kept at the temperature for 1 h. After being cooled naturally to room temperature, the obtained black fibers were re-heated to 200 °C in air and kept at the temperature for 1.5 h to allow any cobalt-based NPs to transform to the Co_3O_4 phase.[23]

It is noteworthy that the precise control of Co_3O_4 loading in the final carbonized hybrid material is not straightforward due to the partial decomposition of PAN during the carbonization process. The decomposition content of PAN may vary notably to the change in the polymer to cobalt acetate ratio or the following thermal treatment temperature. Such change may insignificantly affect the load of Co_3O_4 in the obtained particles-on-fiber hybrids; however, the impact on its electrocatalytic activity can be notably high. For instance, the hybrid Co_3O_4-CNFs obtained from the precursors with a weight ratio (PAN/cobalt acetate) of 8 : 1 or 16 : 1 show inferior ORR and OER activities as compared to that of the C–CoPAN900 obtained from the 4 : 1 precursor (Fig. S6, ESI†). The TGA results suggest the load of Co_3O_4 in these 2 cases is just slightly lower (14.8% and 11.6%). One can comfortably conclude that the electrochemical catalytic activity of the hybrid CNF will be further improved with a further increase in the Co_3O_4 load; however, too high loading of Co_3O_4 NPs will significantly compromise the mechanical strength of the obtained hybrid Co_3O_4-CNF mat. As the ratio of PAN to cobalt acetate in the starting precursor solution is increased to 1 : 1, the resultant hybrid CNF mat becomes rather fragile and can no longer serve directly as an integrated electrode, which is out of the scope of the present study. Nevertheless, full control over experiment parameters and the optimization of the mixture ratio as well as the heating conditions are crucial for any further improvement on the performance of these hybrid CNF mat electrode, which remains as one of our ongoing efforts.

4.2 Material characterizations

The morphology of the electrospun fibers were characterized using a JMF 6700F scanning electron microscope (SEM) and a Philips CM300 transmission electron microscope (TEM). The energy dispersive X-ray (EDX) spectrum and elemental mapping were recorded with an EDS detector (Oxford INCA) equipped on the SEM. The Raman spectrum data was collected using a WITEC CRM200 Raman system with light source of He–Ne laser of λ = 633 nm. Thermogravimetric analysis (TGA) was performed on TGA Q500 (TA instruments) under an air atmosphere. X-ray photoelectron spectroscopy (XPS) data was collected with a Theta Probe electron spectrometer (VG ESCALAB200i-XL, Thermo Scientific). The binding energies were calibrated using C 1s peak at 285.0 eV.

4.3 Electrochemical measurements

Cyclic voltammetry (CV), linear sweep voltammetry (LSV) and rotating disk electrode (RDE) measurements were carried out on an Autolab potentiostat/galvanostat (PGSTAT302N) station in 0.1 M KOH aqueous electrolyte saturated by O_2 or N_2. Pt foil and Ag/AgCl in 3 M KCl were used as the counter electrode and reference electrode, respectively. The working electrode was prepared as follows: (i) dispersing the active material (~5 mg for C–CoPAN900) in 1 mL of aqueous mixture containing 200 μL Nafion (5 wt% aqueous solution, Sigma Aldrich) *via* sonication for at least 30 min to form a homogeneous catalyst ink solution; (ii) applying an appropriate volume of such a solution carefully onto a glassy carbon electrode (GC, 5 mm in diameter, Metrohm); (iii) drying it in air naturally to obtain a uniform thin film. The catalyst loadings for C–CoPAN900 and Pt/C (20 wt% of platinum on carbon black) were ~0.3 mg cm^{-2} and ~0.12 mg cm^{-2}, respectively.

The electron transfer numbers (n) per O_2 involved in ORR were calculated from the slopes of the Koutecky–Levich plots according to the following equations:

$$\frac{1}{j} = \frac{1}{j_L} + \frac{1}{j_K} = \frac{1}{B\omega^{1/2}} + \frac{1}{j_K} \quad (1)$$

$$B = 0.2nFC_0D_0^{2/3}\nu^{-1/6} \quad (2)$$

$$j_K = nFkC_0 \quad (3)$$

where j is the measured current density, j_K and j_L are the kinetic limiting and diffusion limiting current densities, respectively, ω is the angular velocity, F is Faraday constant, C_0 is the bulk concentration of O_2, D_0 is the diffusion coefficient of O_2, ν is the kinematic viscosity of the electrolyte and k is the electron-transfer rate constant.[22]

4.4 Zn-air battery (ZnAB) assembly and tests

ZnABs were assembled with a home-made Zn-air cell (Fig. S4A†) using either a conventionally prepared catalyst cathode or an integrated electrode of the carbonized electrospun nanofiber mat. The battery performance was evaluated by continuous discharge–charge experiments performed under ambient air conditions (oxygen supplied only from the environment, without additional O_2 sources[6]) using an alkaline aqueous electrolyte of 6 M KOH (containing 0.2 M $ZnCl_2$ to facilitate the reversible Zn electrochemical reactions by forming zincate[6]) and a polished zinc plate as the anode (Fig. S4A†). The current density used for the battery test was normalized by the geometric surface area of the catalyst film.

To prepare the cathode by the conventional method, the catalyst ink solution of C–CoPAN900 described in electrochemical experiments was loaded onto a carbon paper.[6,14] To control the amount and the deposition area of the catalyst, a piece of Parafilm® with pre-punched hole (12.7 mm in diameter) was firmly attached onto the carbon paper to create a catalyst "reservoir"; subsequently, the required amount of catalyst ink was specifically deposited within the "reservoir" and allowed to form a well-defined and uniform catalyst layer after drying (Fig. S4B†). In this way, the catalyst mass loading and area could be well controlled. Similarly, an air cathode using the commercial Pt/C catalyst was also prepared for comparison purposes. The catalyst loading was 1.0 mg cm^{-2} for all catalyst electrodes prepared by the conventional method. For the integrated electrode proposed in this work, the C–CoPAN900 fiber mat was directly used as the catalyst air cathode without any additional preparation steps or additives.

Acknowledgements

This research was conducted under the project of IMRE/12-2P0504, which is part of the Advanced Energy Storage Research Programme, supported by the Science and Engineering Research Council (SERC) of A*STAR (Agency for Science, Technology and Research). The authors thank Dr Zhang Zheng and Ms June Ong Lay Ting (IMRE) for the help in XPS measurement.

Notes and references

1 K. M. Abraham and Z. Jiang, *J. Electrochem. Soc.*, 1996, **143**, 1.
2 F. Y. Cheng and J. Chen, *Chem. Soc. Rev.*, 2012, **41**, 2172.
3 Y. Li and H. Dai, *Chem. Soc. Rev.*, 2014, **43**, 5257.
4 L. J. Hardwick and P. G. Bruce, *Curr. Opin. Solid State Mater. Sci.*, 2012, **16**, 178.
5 D. Linden and T. B. Reddy, *Handbooks of Batteries*, McGraw-Hill, 2001.
6 Y. Li, M. Gong, Y. Liang, J. Feng, J.-E. Kim, H. Wang, G. Hong, B. Zhang and H. Dai, *Nat. Commun.*, 2013, **4**, 1085.
7 Z. Peng, S. A. Freunberger, Y. Chen and P. G. Bruce, *Science*, 2012, **337**, 563.
8 P. G. Bruce, S. A. Freunberger, L. J. Hardwick and J.-M. Tarascon, *Nat. Mater.*, 2012, **11**, 19.
9 J.-S. Lee, S. T. Kim, R. Cao, N.-S. Choi, M. Liu, K. T. Lee and J. Cho, *Adv. Energy Mater.*, 2011, **1**, 34.
10 P. Arora and Z. M. Zhang, *Chem. Rev.*, 2004, **104**, 4419.
11 A. Morozan, B. Jousselme and S. Palacin, *Energy Environ. Sci.*, 2011, **4**, 1238.
12 C. Zhu and S. Dong, *Nanoscale*, 2013, **5**, 10765.
13 Z. Chen, J.-Y. Choi, H. Wang, H. Li and Z. Chen, *J. Power Sources*, 2011, **196**, 3673.
14 G. Du, X. Liu, Y. Zong, T. S. A. Hor, A. Yu and Z. Liu, *Nanoscale*, 2013, **5**, 4657.
15 F. W. T. Goh, Z. Liu, X. Ge, Y. Zong, G. Du and T. S. A. Hor, *Electrochim. Acta*, 2013, **114**, 598.
16 Y. Liang, Y. Li, H. Wang and H. Dai, *J. Am. Chem. Soc.*, 2013, **135**, 2013.
17 J. H. Kim and Y. C. Kang, *Nanoscale*, 2014, **6**, 4789.
18 S. Mao, Z. H. Wei, T. Z. Huang, Y. You and J. H. Chen, *Energy Environ. Sci.*, 2014, **7**, 609.
19 Y. L. Zhai, C. Z. Zhu, E. K. Wang and S. J. Dong, *Nanoscale*, 2014, **6**, 2964.
20 G. Q. Zhang, B. Y. Xia, X. Wang and X. W. Lou, *Adv. Mater.*, 2014, **26**, 2408.
21 Y. Liang, H. Wang, P. Diao, W. Chang, G. Hong, Y. Li, M. Gong, L. Xie, J. Zhou, J. Wang, T. Z. Regier, F. Wei and H. Dai, *J. Am. Chem. Soc.*, 2012, **134**, 15849.
22 Y. Liang, Y. Li, H. Wang, J. Zhou, J. Wang, T. Regier and H. Dai, *Nat. Mater.*, 2011, **10**, 780.
23 D.-H. Ha, M. A. Islam and R. D. Robinson, *Nano Lett.*, 2012, **12**, 5122.
24 E. Yoo and H. Zhou, *ACS Nano*, 2011, **5**, 3020.
25 J.-S. Lee, G. S. Park, H. I. Lee, S. T. Kim, R. Cao, M. Liu and J. Cho, *Nano Lett.*, 2011, **11**, 5362.
26 R. Black, J.-H. Lee, B. Adams, C. A. Mims and L. F. Nazar, *Angew. Chem., Int. Ed.*, 2013, **52**, 392.
27 J.-J. Xu, D. Xu, Z.-L. Wang, H.-G. Wang, L.-L. Zhang and X.-B. Zhang, *Angew. Chem., Int. Ed.*, 2013, **52**, 3887.
28 S. Liu, Z. Wang, C. Yu, H. B. Wu, G. Wang, Q. Dong, J. Qiu, A. Eychmueller and X. W. Lou, *Adv. Mater.*, 2013, **25**, 3462.
29 M. Prabu, K. Ketpang and S. Shanmugam, *Nanoscale*, 2014, **6**, 3173.
30 Y. Chen, F. Li, D.-M. Tang, Z. Jian, C. Liu, D. Golberg, A. Yamada and H. Zhou, *J. Mater. Chem. A*, 2013, **1**, 13076.
31 F. Li, Y. Chen, D.-M. Tang, Z. Jian, C. Liu, D. Golberg, A. Yamada and H. Zhou, *Energy Environ. Sci.*, 2014, **7**, 1648.

32 M. Zhang, E. Uchaker, S. Hu, Q. Zhang, T. Wang, G. Cao and J. Li, *Nanoscale*, 2013, **5**, 12342.
33 L. Zhang, F. Zhang, G. Huang, J. Wang, X. Du, L. Qin and L. Wang, *J. Power Sources*, 2014, **261**, 311.
34 J.-M. Kim, H.-S. Park, J.-H. Park, T.-H. Kim, H.-K. Song and S.-Y. Lee, *ACS Appl. Mater. Interfaces*, 2014, **6**, 12789.
35 D. U. Lee, J.-Y. Choi, K. Feng, H. W. Park and Z. Chen, *Adv. Energy Mater.*, 2014, **4**, 1301389.
36 T. H. Hwang, Y. M. Lee, B.-S. Kong, J.-S. Seo and J. W. Choi, *Nano Lett.*, 2012, **12**, 802.
37 T. H. Hwang, D. S. Jung, J.-S. Kim, B. G. Kim and J. W. Choi, *Nano Lett.*, 2013, **13**, 4532.
38 P. Chen, T.-Y. Xiao, Y.-H. Qian, S.-S. Li and S.-H. Yu, *Adv. Mater.*, 2013, **25**, 3192.
39 G.-L. Tian, M.-Q. Zhao, D. Yu, X.-Y. Kong, J.-Q. Huang, Q. Zhang and F. Wei, *Small*, 2014, **10**, 2251.
40 X.-C. Dong, H. Xu, X.-W. Wang, Y.-X. Huang, M. B. Chan-Park, H. Zhang, L.-H. Wang, W. Huang and P. Chen, *ACS Nano*, 2012, **6**, 3206.
41 J. Wang, J. Zhou, Y. Hu and T. Regier, *Energy Environ. Sci.*, 2013, **6**, 926.
42 K. Gong, F. Du, Z. Xia, M. Durstock and L. Dai, *Science*, 2009, **323**, 760.
43 L. Qu, Y. Liu, J.-B. Baek and L. Dai, *ACS Nano*, 2010, **4**, 1321.
44 G. Wang, X. Shen, J. Horvat, B. Wang, H. Liu, D. Wexler and J. Yao, *J. Phys. Chem. C*, 2009, **113**, 4357.
45 L. Wu, H. Feng, M. Liu, K. Zhang and J. Li, *Nanoscale*, 2013, **5**, 10839.
46 M. J. Escudero, L. Mendoza, M. Cassir, T. Gonzalez and L. Daza, *J. Power Sources*, 2006, **160**, 775.
47 L. Fu, K. Tang, K. Song, P. A. van Aken, Y. Yu and J. Maier, *Nanoscale*, 2014, **6**, 1384.
48 Y. Li, Z. Huang, K. Huang, D. Carnahan and Y. Xing, *Energy Environ. Sci.*, 2013, **6**, 3339.
49 R. Silva, D. Voiry, M. Chhowalla and T. Asefa, *J. Am. Chem. Soc.*, 2013, **135**, 7823.
50 J.-S. Lee, T. Lee, H.-K. Song, J. Cho and B.-S. Kim, *Energy Environ. Sci.*, 2011, **4**, 4148.
51 S. Zhu, Z. Chen, B. Li, D. Higgins, H. Wang, H. Li and Z. Chen, *Electrochim. Acta*, 2011, **56**, 5080.
52 T.-H. Yang, S. Venkatesan, C.-H. Lien, J.-L. Chang and J.-M. Zen, *Electrochim. Acta*, 2011, **56**, 6205.
53 Z. Chen, A. Yu, R. Ahmed, H. Wang, H. Li and Z. Chen, *Electrochim. Acta*, 2012, **69**, 295.
54 X. Zhou, L.-J. Wan and Y.-G. Guo, *Small*, 2013, **9**, 2684.
55 C.-L. Zhang and S.-H. Yu, *Chem. Soc. Rev.*, 2014, **43**, 4423.
56 X. Lu, C. Wang and Y. Wei, *Small*, 2009, **5**, 2349.

